Co-published by
Institute of Fluid-Flow Machinery
Polish Academy of Sciences
Committee on Thermodynamics and Combustion
Polish Academy of Sciences

http://www.imp.gda.pl/archives-of-thermodynamics/

Heat Transfer Analysis of a Longitudinal Fin Attached to a Beta-Type Stirling Engine

Ishita Rai*, Rajeev Kumar

Birla Institute of Technology, Mesra 835215, India
*Corresponding author email: phdme10006.21@bitmesra.ac.in

Received: 01.01.2025; revised: 31.05.2025; accepted: 26.07.2025

Abstract

Our proposed model is a highly non-linear parabolic heat transfer equation for the longitudinal fin with an insulated fin tip, temperature dependent thermal conductivity, and internal heat generation in the transient condition. The research comprises several components, namely, a discussion of the longitudinal fin heat transfer model, its solution, the validation of the numerical scheme and solution analysis, and finally, the influence of fin attachment on the system. Mathematical formulations were developed to represent identified fin parameters. This enables us to investigate further their variation patterns, therefore making future modelling easy as well as providing a better understanding of their applicability in developing energy storage systems.

Keywords: Stirling engine; Longitudinal fin; FERK (4,5) scheme; Heat transfer; Thermoelectric generator

Vol. 46(2025), No. 3, 51–60; doi: 10.24425/ather.2025.156578

Cite this manuscript as: Rai, I., & Kumar, R. (2026). Heat Transfer Analysis of a Longitudinal Fin Attached to a Beta – Type Stirling Engine. *Archives of Thermodynamics*, 46(3), 51−60.

1. Introduction

Stirling engines were developed in 1816 by Rev. Robert Stirling. They work in a closed regenerative cycle in which a working fluid is externally heated. The cyclic compression and expansion of fluid is utilised by the piston to produce power. As a result of its multi-fuel functionality, it has a wide range of applications, Yang et al. [1]. Based on the location of the piston and cylinder configuration, these engines are classified into three types: Alpha, Beta and Gamma type Stirling Engines. Other classifications include free-piston Stirling engines, double-acting Stirling engines, thermal lag Stirling engines, multi-cylinder liquid-piston Stirling engines, pulse tube Stirling engines, and thermoacoustic Stirling engines, etc. [2]. Stirling engines have been designed in a wide range from large marine engines to the nanoscale [3,4]. Its applications are prophesied from outer space to the human heart [3,5].

It has been found that although the Stirling cycle claims to have an efficiency on the same scale as the Carnot cycle, its practical application does not have that high efficiency. Simultaneous heating and cooling come as the biggest challenge, in maintaining the desired temperature difference.

The first analytical model for the Stirling engine was developed by Schmidt in 1871 [6]. Building on this, researchers like Finkelstein et al. [7], Walker [8], and Kirkley [9] explored optimal phase angles and swept volume ratios for alpha, beta, and gamma types of Stirling engines and refrigerators. In their findings, it appears that the β-type Stirling engine produces the high-

Nomenclature

A_c – cross-sectional area of fin, m^2
A_m – dimensionless amplitude of base temperature
c – specific heat of fin material, J/(kg·K)
Fo – Fourier number
f – frequency related to engine operating speed
G – internal heat generation coefficient or generation number
h – Newton's cooling constant, W/(m^2·K)
$k(T)$– thermal conductivity, W/(m·K)
L – length of the fin, m
N – thermogeometric fin parameter
P – fin perimeter, m
q – internal heat generation, W/m^2
Re – Reynolds number,
T – temperature, K
t – time, s
x – space co-ordinate, m

Greek symbols

ε – internal heat generation parameter, 1/K
θ – local fin temperature
X – coordinate space
ε_G – associate coefficient of internal heat generation
ρ – density of fin material, kg/m^3
ω – periodicity, s^{-1}
Ω – non-dimensional periodicity
Φ – phase shift

Subscripts and Superscripts

b – base
∞ – ambient
m – mean

Abbreviations and Acronyms

FERK – finite element Runge-Kutta
ERS – energy recovery systems
TEG – thermoelectric generator

est indicated work, while the gamma-type yielded the lowest. Further studies confirmed that β-types are more efficient than alpha or gamma types under similar conditions [10].

In addition to thermodynamic models, a three-dimensional CFD approach can be used to analyse the Stirling engine. Mahkamov [11] conducted a CFD simulation for a solar powered Striling engine, while Hung and Cheng [12] used CFD methods to predict flow, pressure, and thermal fields in a piston-cylinder assembly. Although CFD methods provide detailed information, they are more time-consuming and computationally intensive than thermodynamic models [13].

The performance of the Stirling engine depends on the temperature difference between the hot and cold regions. Once the engine starts to work, the heated working fluid is forced to expand and moves towards the colder region. This exchange of working fluid between the cold region and hot region, if remains unchecked, will generate a uniform temperature profile throughout the cylinder and will seize the engine operation. Fins are attached to perform this task efficiently. Kumaravelu et al. [14] studied the Stirling engine performance without and with different fin configuration models. They found that engine efficiency without fin attachment is 10.26%; with circular fins attached, its efficiency is 14.41%, with pin fins attached, its efficiency is 16.64%, and when rectangular fins are attached, its efficiency is 19.03%. They concluded that rectangular fins are more efficient due to their larger surface area. Since fin properties and geometry vary, mathematical studies are needed to assess their impact on cooling efficiency. In Stirling engines, since there are no valves or ports for induction or exhaust, energy is transferred through cylinder walls or heat exchangers. Thus, fins play a crucial role in indirect heat rejection to the surroundings. Numerous studies have modelled heat transfer in fins [14–18].

Energy recovery systems (ERS) such as a thermoelectric generator (TEG) work on the principle of the Seebeck effect. When combined with Stirling engines, TEG provides an opportunity to convert waste heat into additional electric power. It has been found by Faraj et. al. [19] that attaching fins to a 40×40 cm^2 flat plate TEG system generates 3.8 W of electrical power in combination with solar radiation of 2000 W/m^2 and reduces one ton of carbon dioxide emission yearly. Energy recovery systems are strategies used to recover system energy that would otherwise be squandered. In recent years, ERS has been regarded as a cost-effective choice for increasing efficiency, and as a result, the potential advantages of those systems are being fully utilised [20]. Ideally, when applying ERS, energy must be utilised continuously, and the efficiency gain must be significant in all conditions. Waste energy from the Stirling engine can be harvested in developing ERS utilising the fins attached to its colder section. For a waste heat recovery system for power generation, in a lower temperature range, Chen et al. [21] suggested adding fins within a range of 0–27 items, which significantly enhances heat transport and the performance of thermoelectric modules (TEMs). At Re = 10 and 100, a perfect number of fins is 21, whereas it is 27 at Re =1000. At Re =1000, the highest overall power generated is 0.411 W, and the average efficiency of conversion is 0.95%. When compared to TEMs without fins, these figures represent 105.5% and 43.94% enhancements, respectively.

1.1. Present contribution

Our proposed model is a highly non-linear parabolic heat transfer equation for the longitudinal fin with an insulated fin tip, temperature dependent thermal conductivity and internal heat generation. It is a realistic model of the longitudinal fin compared to the existing model. This type of model is for the first time used in the transient and highly non-linear conditions in the fin material. FERK(4,5) scheme is used for the solution of our non-linear parabolic heat transfer equation. The research comprises six components. The first component is to discuss longitudinal fin heat transfer modelling. The second section contains a system description; the third section concentrates on solving the problem. In the fourth section, the validation analysis of the numerical scheme has been presented. The fifth section discusses the influence of parameters on the system. The sixth section is devoted to final conclusions.

A key gap identified in the available research literature is the absence of transient heat transfer modelling of a fin attached to the cold region of a β-type Stirling engine. The given model represents a realistic situation as:

1. the mathematical formulation was developed to represent identified fin parameters; this enables us to investigate further their variation patterns, therefore making future modelling easy as well as providing a better understanding of their applicability in developing energy storage systems;
2. the model provides a mathematical backup to the study of heat transfer through the fin.

2. System description

We consider a system consisting of a β-type Stirling heat engine operating between a heat source and a heat sink at the temperatures T_H and T_L, respectively (Fig. 1). Near the wall area, hydrodynamically non-slip walls satisfying the temperature continuity and heat flux continuity at both sides of the wall are applied to accurately simulate the thermo-hydraulic output [14]. The cold region includes longitudinal fins (Fig. 2).

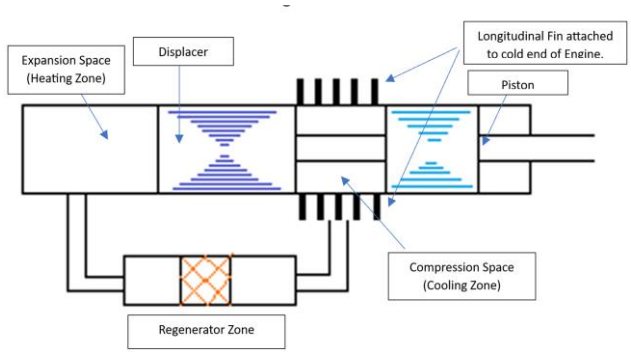

Fig. 1. Fin attachment to "cold region" of β-type Stirling engine.

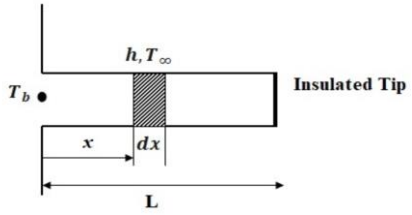

Fig. 2. Schematic geometry of the longitudinal fin.

For boundary conditions, a conjugated heat transfer was assumed for the fin fluid/solid wall [14]. The temperature at the base of the longitudinal fin varies cyclically due to cyclic changes in the temperature of the working gas, within the cylinder. The area of the cross-section of the fin is A_c, thickness b, length L, and perimeter P. Width is dominated by length, i.e. $b/L \ll 1$. The amount of heat dissipated from the tip can be discounted to be zero as the tip area is negligible in comparison to the total fin area [22,23]. When heat is generated inside the fin by utilising an external energy source, an opportunity for dynamic thermal management, hybrid thermal circuit and energy recovery is observed. The internal heat generation term, q, has been added in the analysis to cover such scenarios. The physical properties of the longitudinal fin and system assumptions are considered as follows:

1. A transient state is assumed.
2. The fin material has a temperature dependent thermal conductivity.
3. The density of longitudinal fin material is ρ, and the specific heat is c.
4. Fin is assumed to have a uniform cross-sectional area.
5. Conduction is assumed to be in one dimension.
6. We assume a constant convective heat transfer coefficient h. The convection is assumed to happen at the fin surface exposed to the surrounding only.
7. A local fin temperature-dependent internal heat generation is denoted by q.
8. Temperature variation at the fin base is assumed to be a function of engine dynamic characteristic, phase angle Φ.

2.1. Mathematical Formulation

Under the above assumptions, the differential equations governing heat transfer in the longitudinal fin come out as [23–25]:

$$\rho c \frac{\partial T}{\partial t} = \frac{\partial}{\partial x}\left\{k(T)\frac{\partial T}{\partial x}\right\} - \frac{hP}{A_c}(T - T_\infty) + q(T), \qquad (1)$$

where:

$$q(T) = q_\infty\{1 + \varepsilon(T - T_\infty)\},$$

$$k(T) = k_\infty\{1 + \alpha(T - T_\infty)\}.$$

The initial conditions are assumed as:

$$T(x, o) = T_\infty, \qquad (2)$$

and the temperature at the base of the longitudinal fin is given by [24–27]:

$$T(0, t) = T_{b,m} + A_m\left(T_{b,m} - T_\infty\right)\cos(\omega t + \Phi), \qquad (3)$$

where $T_{b,m}$ is the mean base temperature of the cold side during the cycle. A_m is the dimensionless amplitude of the base temperature and $\omega = 2\pi ft$, where frequency f is directly related to the engine operating speed. Time in seconds is represented by t. $\Phi \in [0, 2\pi]$ represents the phase shift, covering the one complete cycle of the cosine wave.

In the actual phenomenon, the temperature profile decreases with respect to x, see Fig. 2. We consider the insulated tip [22,23] in our assumption, so at $x = L$, we use the condition:

$$\frac{\partial T}{\partial x}(L, t) = 0. \qquad (4)$$

By introducing non-dimensional variables and similarity criteria as follows:

$$\theta = \frac{T - T_\infty}{T_{b,m} - T_\infty}, \quad X = \frac{x}{L}, \quad \mathrm{Fo} = \frac{k_\infty t}{\rho c L^2}, \quad N^2 = \frac{hPL^2}{k_\infty A_c}, \quad \Omega = \frac{\rho c L^2 \omega}{k_\infty} \qquad (5)$$

$$G = \frac{q_\infty A_c}{hP(T_{b,m} - T_\infty)}, \quad \varepsilon_G = \varepsilon\left(T_{b,m} - T_\infty\right), \quad \beta = \alpha\left(T_{b,m} - T_\infty\right),$$

the system of Eqs. (1)–(4), in a non-dimensional form reduces to:

$$\frac{\partial\theta(X,\mathrm{Fo})}{\partial\mathrm{Fo}} = (1+\beta\theta)\frac{\partial^2\theta(X,\mathrm{Fo})}{\partial X^2} + \beta\left(\frac{\partial\theta}{\partial X}\right)^2 - N^2(1-G\varepsilon_G)\theta(X,\mathrm{Fo}) + N^2G, \quad (6)$$

$$\theta(X,0) = 0, \quad (7)$$

$$\theta(0,\mathrm{Fo}) = 1 + A_m\cos(\Omega\mathrm{Fo}+\Phi), \quad (8)$$

$$\frac{\partial\theta(1,\mathrm{Fo})}{\partial X} = 0. \quad (9)$$

3. Solution of the problem

The hybrid numerical scheme combining two techniques has been developed. The first one is discretization in space coordinates, and the other one is the Runge-Kutta (4,5) scheme. We discretised the space coordinate [0, 1] into n+1 equal size subintervals of length h. Using finite differences, the boundary value problem (Eqs. (6)–(9)) reduces to an initial value problem of the system of first-order non-linear ordinary differential equations, as follows:

$$\frac{\mathrm{d}\theta_1}{\mathrm{dF_o}} = -\left[\frac{2}{h^2} + N^2(1-\varepsilon_G G)\right]\theta_1 + \frac{\theta_2}{h^2} + \frac{\beta}{h^2}\left(-2\theta_1^2 + \theta_1\theta_2 + \frac{1}{4}\theta_2^2\right) + \frac{\beta}{h^2}\left(\theta_1 - \frac{1}{2}\theta_2\right)(1 + A_m\cos(\Omega\mathrm{Fo}+\Phi)) + \frac{(1+A_m\cos(\Omega\mathrm{Fo}+\Phi))}{h^2} + \frac{\beta}{4h^2}(1 + A_m\cos(\Omega\mathrm{Fo}+\Phi))^2 + N^2G, \quad (10)$$

$$\frac{d\theta_i}{d\mathrm{Fo}} = \frac{\theta_{i-1}}{h^2} - \left[\frac{2}{h^2} + N^2(1-\varepsilon_G G)\right]\theta_i + \frac{\theta_{i+1}}{h^2} + \frac{\beta}{h^2}(\theta_i\theta_{i+1} - 2\theta_i^2 + \theta_i\theta_{i-1}) + \frac{\beta}{4h^2}(\theta_{i+1}^2 - 2\theta_{i+1}\theta_{i-1} + \theta_{i-1}^2) + N^2G, \quad i = 2,\dots,n-1, \quad (11)$$

$$\frac{d\theta_n}{d\mathrm{Fo}} = \frac{\theta_{n-1}}{h^2} - \left[\frac{2}{h^2} + N^2(1-\varepsilon_G G)\right]\theta_n + \frac{\beta}{h^2}\left[-2\theta_n^2 + \theta_n\theta_{n-1}\right] + \frac{\beta}{4h^2}\theta_{n-1}^2 + N^2G + \frac{1}{h^2}\left[1 + \beta\theta_n - \frac{\alpha}{2}\theta_{n-1}\right]\theta_{n+1} + \frac{\beta}{4h^2}\theta_{n+1}^2, \quad (12)$$

under the initial condition:

$$\theta_i(0) = 0. \quad (13)$$

To calculate the tip temperature of the fin, using a three-point formula, we write:

$$\theta_{n+1} = \frac{1}{21}(13\theta_n + 17\theta_{n-1} - 9\theta_{n-2}). \quad (14)$$

The highly non-linear system of first-order non-linear ordinary differential equations (10)–(12) under the initial condition (13) is solved using the Runge-Kutta (4,5) technique. For all computational work, MATLAB-R2024 software is utilised.

3.1. Exact solution

For the validation of the proposed numerical scheme of the problem, an analytical solution is required. When we assume the associated coefficient of thermal conductivity β =0, and the boundary condition at the base of the fin as constant in Eqs. (6) and (8), then the proposed model of heat transfer is changed into the following form:

$$\frac{\partial\theta(X,\mathrm{Fo})}{\partial\mathrm{Fo}} = \frac{\partial^2\theta(X,\mathrm{Fo})}{\partial X^2} - N^2(1-G\varepsilon_G)\theta(X,\mathrm{Fo}) + N^2G, \quad (15)$$

$$\theta(X,0) = 0, \quad (16)$$

$$\theta(0,\mathrm{Fo}) = 1, \quad (17)$$

$$\frac{\partial\theta(1,\mathrm{Fo})}{\partial X} = 0. \quad (18)$$

Applying the Laplace transform technique, the exact solution of the system of Eqs. (15)–(18) comes out as follows:

$$\theta(X,\mathrm{Fo}) = \frac{\cosh\left(\sqrt{N^2(1-G\varepsilon_G)}(X-1)\right)}{\cosh\left(\sqrt{N^2(1-G\varepsilon_G)}\right)} + \sum_{n=1}^{\infty}\frac{(-1)^{n+1}e^{s_n\mathrm{Fo}}(2n-1)\pi\cos(2n-1)\frac{\pi}{2}(X-1))}{s_n} - \frac{G\cosh\left(\sqrt{N^2(1-G\varepsilon_G)}(X-1)\right)}{(1-G\varepsilon_G)\cosh(\sqrt{N^2(1-G\varepsilon_G)})} + \frac{G\,e^{-N^2(1-G\varepsilon_G)\mathrm{Fo}}}{(1-G\varepsilon_G)} + \sum_{n=1}^{\infty}\frac{(-1)^{n+1}4N^2Ge^{s_n\mathrm{Fo}}\cos\left((2n-1)\frac{\pi}{2}(X-1)\right)}{s_n(2n-1)\pi} + \frac{G\left(1-e^{-N^2(1-G\varepsilon_G)\mathrm{Fo}}\right)}{(1-G\varepsilon_G)}, \quad (19)$$

where: $s_n = -(2\pi-1)^2\left(\frac{\pi^2}{4}\right) - N^2(1-G\varepsilon_G);\ n \in N.$

4. Numerical simulation and analysis

In the proposed work, the temperature in the longitudinal fin is studied under the Neumann boundary condition. We consider a temperature dependent thermal conductivity and internal heat generation term, which are functions of local temperature. The FERK (4,5) scheme is applied for the solution of this non-linear parabolic equation to calculate the temperature in the longitudinal fin. The obtained solution is presented in the form of two- and three-dimensional figures. Only the parameters whose values differ from the reference values have been indicated. The selected reference values of dimensionless parameters used to calculate the non-dimensional temperature profile in the longitudinal fin in the finite domain are given in Table 1.

Table 1. The selected reference value of dimensionless parameters.

Parameter	Symbol	Numerical value	Reference
Associated coefficient of thermal conductivity	β	0.2	[28]
Fin parameter	N	1	[28]
Internal heat generation coefficient	G	0.2	[1]
Associated coefficient of internal heat generation	ε_G	0.2	[1]
Dimensionless amplitude of the base temperature	A_m	0	[18]
Dimensionless periodicity	Ω	0	[18]

4.1. Validation of proposed numerical scheme

The FERK (4,5) scheme has been used to obtain a numerical solution of the highly non-linear parabolic equation of heat transfer in the longitudinal fin. By unifying the two techniques, we achieve a greater accuracy with a negligible local error [29,30]. Figure 3 shows a comparative analysis between the FERK (4,5) scheme and the exact analytical solution obtained using the Laplace transform technique. It is found that the developed FERK (4,5) scheme is in excellent agreement with the exact solution. By analysing Fig. 3, we observe a good accuracy with minimum computational complexity, highlighting the advantage of the proposed method [28].

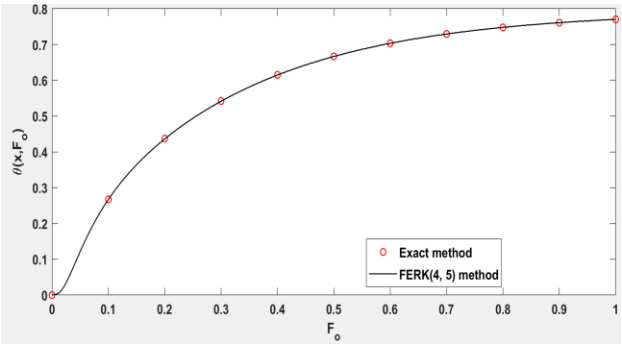

Fig. 3. Comparison between the exact method and FERK (4,5) method.

5. Results and discussion

We discuss the effects of several non-dimensional parameters, affecting heat transfer analysis in the longitudinal fin.

5.1. Effect of Ω and A_m at $\Phi = 0, \pi/2, \pi$

In order to include cyclic temperature variation in the cold wall side, we have introduced three parameters, namely, A_m, dimensionless amplitude of base temperature, Ω, non-dimensional periodicity, and Φ, representing the phase shift, which are included in Eq. (8) [18].

Here A_m represents thermal inertia, reflecting temperature fluctuations, in reference to the mean temperature difference in the cold cylinder wall. In other words, by using A_m in the model, the intensity of thermal oscillations can be quantified. From previous studies [31,32], it was evident that a suitable value of A_m for stable heat transfer in Stirling engines lies between 0.1 and 0.3. Higher values beyond 0.7–1.0 provide a non-ideal behaviour with a thermal lag leading to lower efficiency. Very high values of A_m may cause entropy generation, reducing the network output of the engine. It is evident from Fig. 4 that the non-dimensional temperature increases with the non-dimensional space coordinate as A_m increases, for $\Phi = 0$; the non-dimensional temperature decreases with the non-dimensional space coordinate as A_m increases, for $\Phi = \pi$, and remains constant for $\Phi = \pi/2$. A similar result is obtained by Singh et al. [18] for $\Phi = 0$, as they have studied for $\Phi = 0$, only. Real Stirling engines have thermal inertia: there is a delay between heating the wall and gas temperature rising. Φ can model this delay, accounting for thermal diffusion time. ωt tracks the cyclical evolution of the engine over time. It helps predict when in time the system reaches peak or trough temperatures for optimal heat exchange.

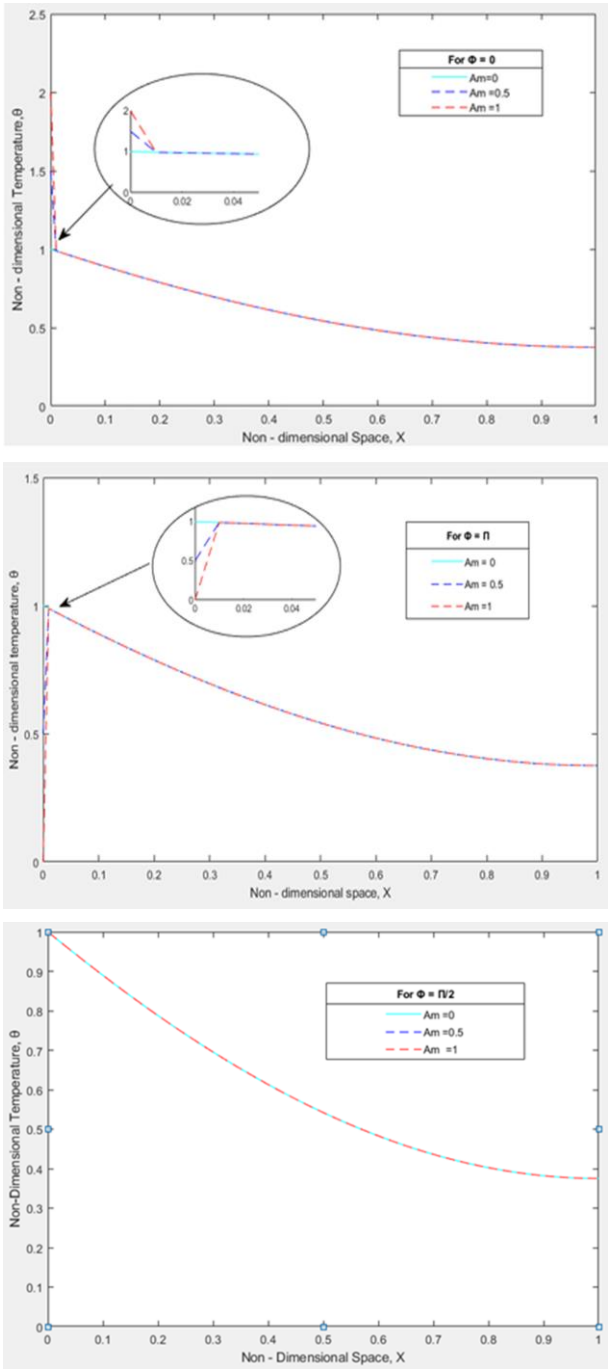

Fig. 4. Variation in dimensionless amplitude of base temperature A_m for fixed values of $\alpha = 1$, $G = 0.2$, $\Omega = 0$, $N = 1$, $\varepsilon_G = 0.2$, Fo = 0.3.

Figure 5 shows the variation of non-dimensional temperature with respect to non-dimensional space coordinates for different values of Ω. It is evident from these figures that θ is the maximum for $\Omega = 0$, and the lowest for $\Omega = 10$, while it lies in between for $\Omega = 100$ when $\Phi = 0$. For $\Phi = \pi$, the non-dimensional temperature θ with respect to non-dimensional space coordinate is the highest when $\Omega = 10$, and the lowest when $\Omega = 0$, and in between for $\Omega = 100$. Further, the non-dimensional temperature, θ, is the highest for $\Omega = 100$ and the lowest for $\Omega = 0$, but in

between when $\Omega = 10$, for $\Phi = \pi/2$. A similar result is obtained by Singh et al. [18] for $\Phi = 0$.

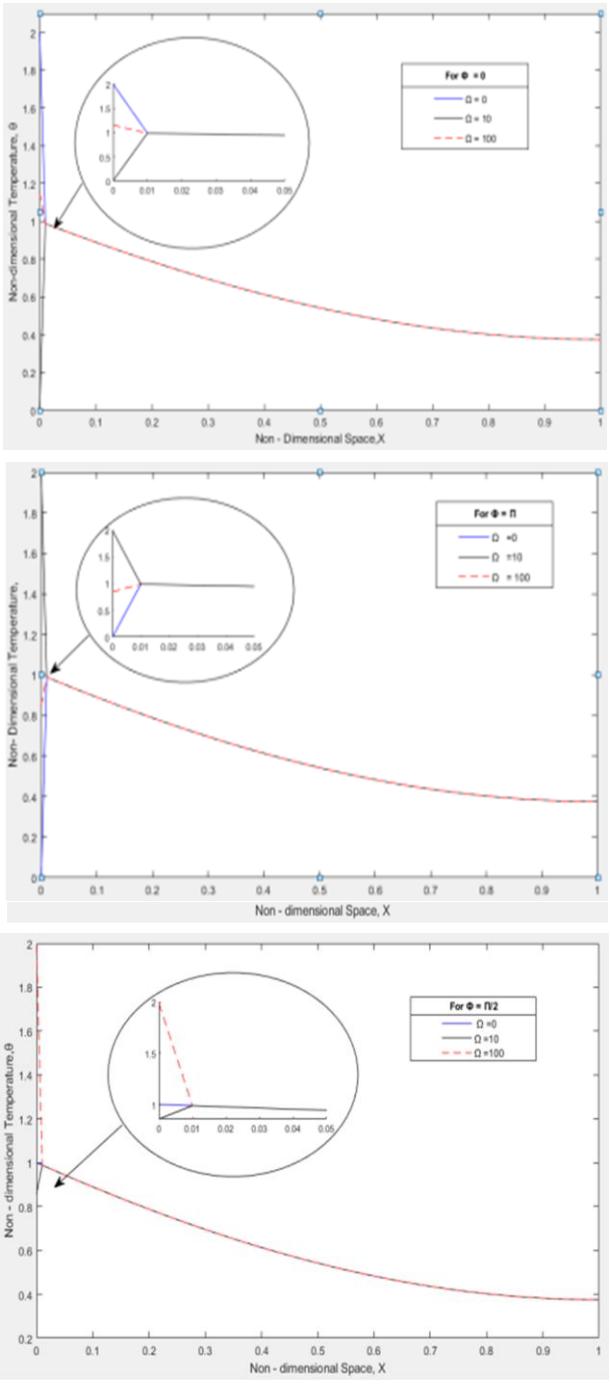

Fig. 5. Variation in non-dimensional periodicity, Ω, for fixed values of $\alpha = 1$, $G = 0.2$, $A_m = 1$, $N = 1$, $\varepsilon_G = 0.2$, Fo = 0.3.

5.2. Effect of Fo and *X*

In Figure 6, we analyse the behaviour of temperature distribution in the longitudinal fin with respect to non-dimensional time, Fo, and non-dimensional space coordinate X. This figure has two components – Figs. 6(a) and 6(b). Figure 6(a) demonstrates the variation of non-dimensional temperature with Fo for different values of X, when $\beta = G = \varepsilon_G = 0.2$ and $N = 1$. We observe from this figure that the non-dimensional temperature increases with Fo but decreases as X increases. Figure 6(b) presents the variation of non-dimensional temperature vs. X for varying Fo, for the same values of fin parameters. It shows that the tip temperature increases as Fo grows, and decreases with time.

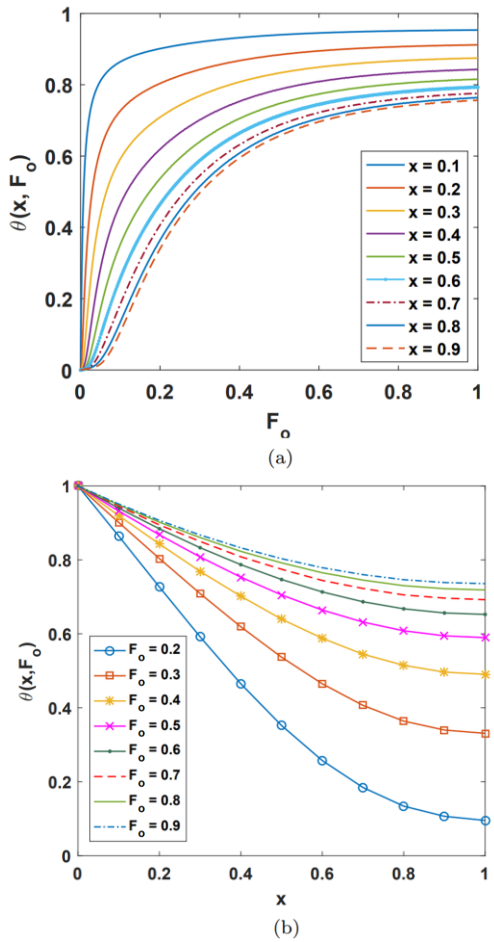

Fig. 6. Temperature distribution in fin vs.: (a) dimensionless time coordinate (F_o), (b) dimensionless space coordinate (x) when $\beta = 0.2$, $N = 1$, $G = 0.2$, and $\varepsilon_G = 0.2$.

5.3. Effect of β

Figure 7 shows the effect of β in two- and three-dimensional coordinate space. It is observed that as β increases, the temperature in the fin increases with Fo and X. This confirms the improved fin conductivity and a more uniform temperature distribution in the fin.

5.4. Effect of *N*

Figure 8 demonstrates the effect of fin parameter N in two- and three-dimensional coordinate systems. We draw Fig. 8(a) as non-dimensional temperature vs. non-dimensional time, Fo, and Fig. 8(b) as non-dimensional temperature vs. non-dimensional space coordinate. It is observed that the temperature in the longitudinal fin increases along Fo and X as the values of N decrease. The fin parameter N increases as convective heat transfer coefficient h, fin perimeter p, and fin length L increase, while the conductivity of fin material, k, and its cross-sectional area A_c decrease. Therefore, it can be concluded that a higher value of N promotes convection, resulting in a better cooling effect.

Thus, a long thin fin will have a prominent temperature difference between both ends. Therefore, it can be concluded that, as N increases, the conductivity pattern deteriorates. In other words, a lower N number denotes thick and short fins, whereas a higher value of N shows a better cooling effect.

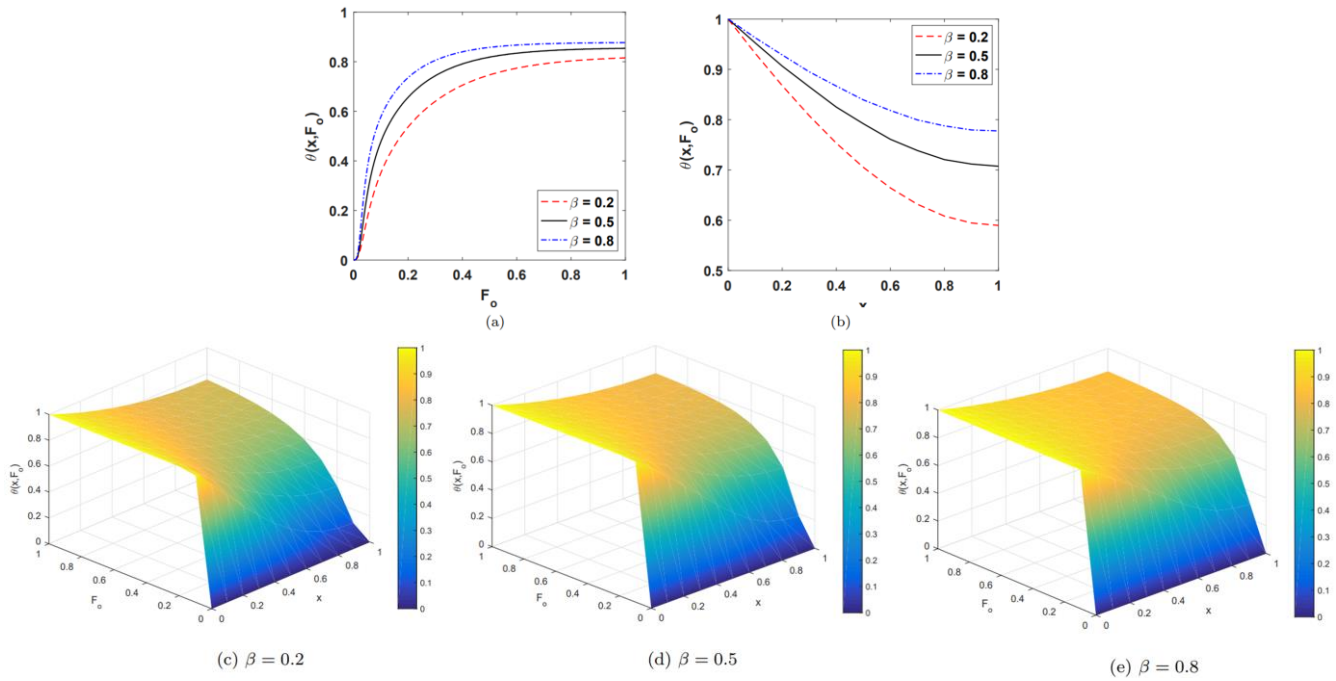

Fig. 7. Temperature distribution in fin vs.: (a) dimensionless time coordinate (F_o), when β =0.2, 0.5, 0.8 and X = 0.5; (b) dimensionless space coordinate (X), when β = 0.2, 0.5, 0.8 and Fo =0.5; (c) Fo and X, when β = 0.2; (d) Fo and X, when β = 0.5; (e) Fo and X, when β =0.8 for fixed numerical values of β = 0.2, N =1, G = 0.2, and ε_G = 0.2.

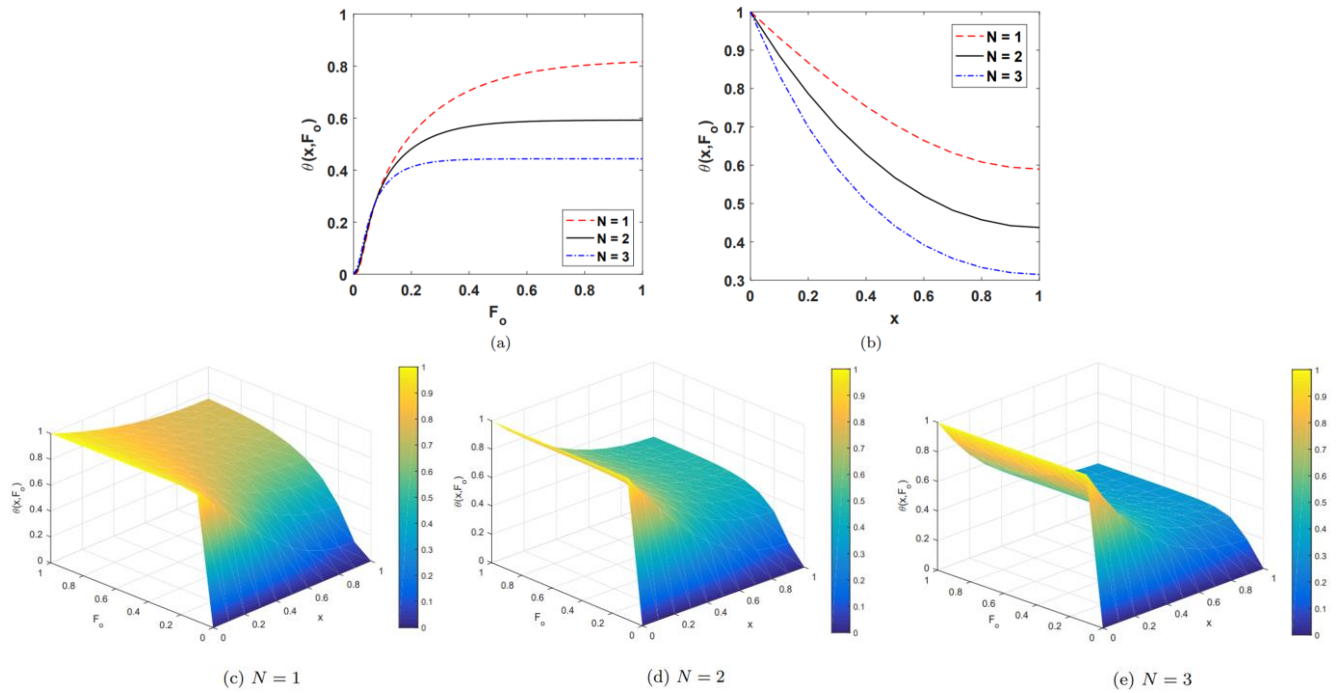

Fig. 8. Temperature distribution in fin vs.: (a) dimensionless time coordinate (F_o), when β =0.2, 0.5, 0.8 and X = 0.5; (b) dimensionless space coordinate (X), when β = 0.2, 0.5, 0.8 and Fo =0.5; (c) Fo and X, when β = 0.2; (d) Fo and X, when β = 0.5; (e) Fo and X, when β =0.8 for fixed numerical values of β = 0.2, N =1, G = 0.2, and ε_G = 0.2.

5.5. Effect of *G*

The effect of the internal heat generation coefficient in two- and three-dimensional coordinate systems is shown in Fig. 9. We draw Fig. 9(a) for the non-dimensional temperature vs. non-dimensional time coordinate, and Fig. 9(b) for the non-dimensional temperature vs. non-dimensional space coordinate. The temperature in the longitudinal fin increases along Fo and X,

with an increase in G. This can be achieved by fin geometry where the cross-sectional area A_c has a smaller value and the perimeter p of the fin is large. This again supports a long fin for better cooling performance.

5.6. Effect of ε_G

Internal heat generation represents the amount of heat generated internally in the fin by consistent heating of the cooling section in the Stirling engine. Figure 10 depicts the effect of the associated coefficient of internal heat generation ε_G in two- and three-dimensional coordinate systems. We draw Fig. 10(a) for the non-dimensional temperature vs. non-dimensional space coordinate. The temperature in the longitudinal fin increases along both Fo and X as the values ε_G increase.

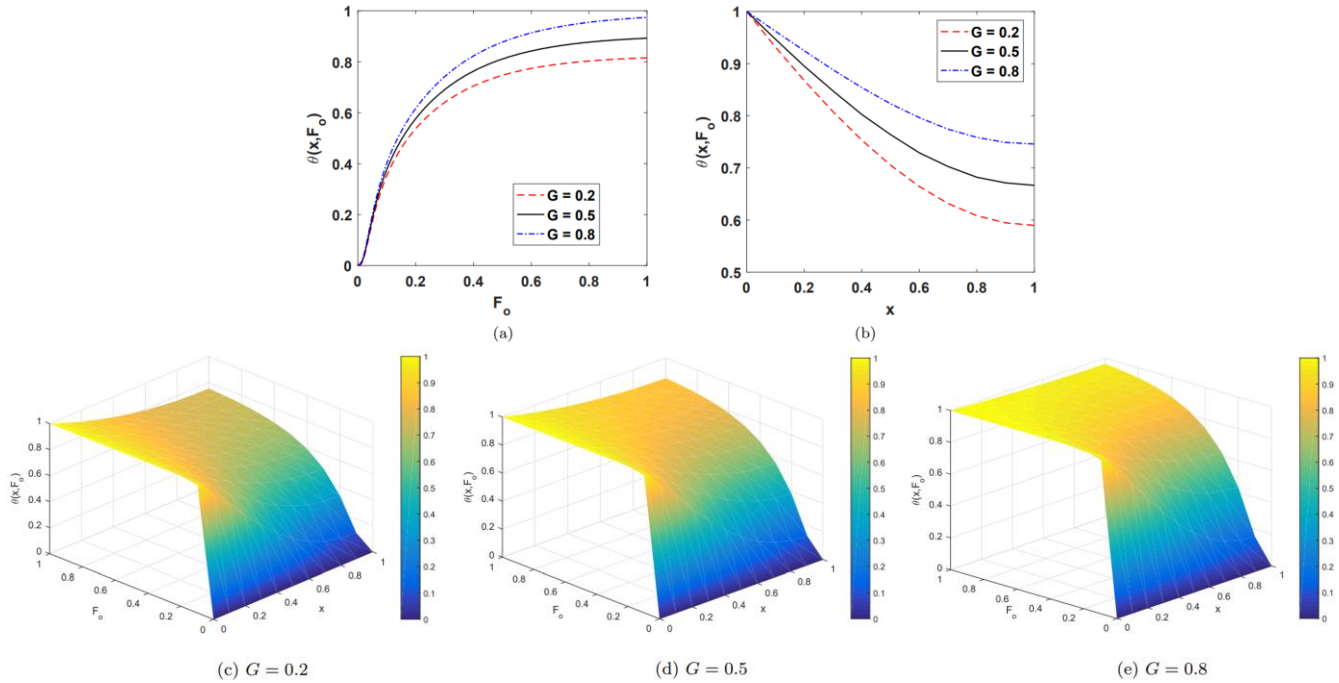

Fig. 9. Plot the temperature distribution in fin vs.: (a) dimensionless time coordinate (Fo), when G = 0.2, 0.5, 0.8; (b) dimensionless space coordinate (x), when G = 0.2, 0.5, 0.8; (c) Fo and x, when G = 0.2; (d) Fo and x, when G = 0.5; (e) Fo and x, when G = 0.8 for fixed numerical values of β = 0.2, N = 1 and ε_G = 0.2.

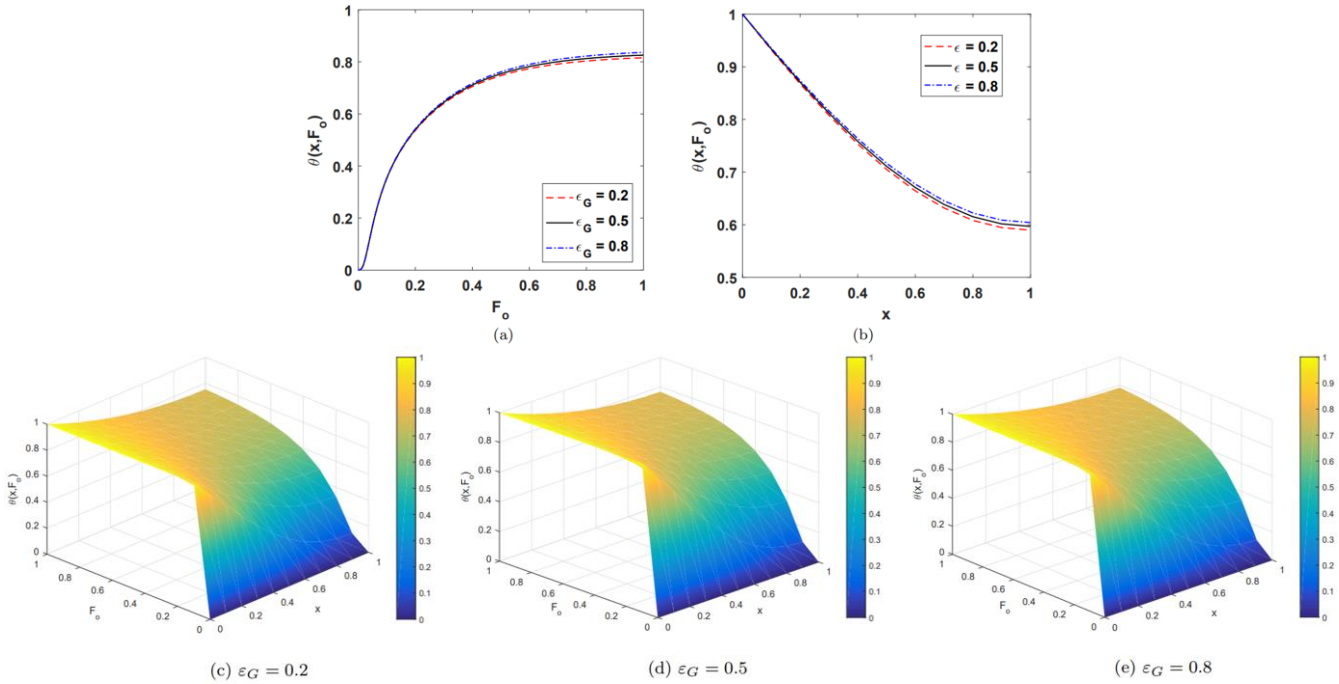

Fig. 10. Plot of the temperature distribution in fin vs.: (a) dimensionless time coordinate (Fo),when ε_G = 0.2, 0.5 , 0.8; (b) dimensionless space coordinate (X), when ε_G = 0.2, 0.5, 0.8; (c) Fo and X, when ε_G = 0.2, (d) Fo and X, when ε_G = 0.5; (e) Fo and X, when ε_G = 0.8 for fixed numerical values of β= 0.2, N =1 and G = 0.2.

6. Conclusions

The goal of this study is to provide validation of the FERK (4,5) method and use this technique for evaluation of the thermal profile in a longitudinal fin attached to a cooler region of a β-type Stirling engine. The wasted heat through the fin is proposed to be utilised by an ERS in generating electricity. The obtained results were analysed for the variability of thermal conductivity and internal heat generation with temperature, thermogeometric fin parameters, and generation number. The important findings are summarised as follows:

1. FERK (4,5) method is justified with exact results in a specific case, and good accuracy is observed.
2. A_m and Ω do not significantly affect temperature distribution in the non-dimensional space over a wide range. For different values of A_m, graphs representing the non-dimensional temperature distribution in non-dimensional space quickly overlap.
3. A suitable value of phase angle Φ was shown by various researchers to be in the range of 60°−80°; As a function of cosine, the range in which Φ varies is from −1 to 1. It has been observed that by varying Φ, a delay can be introduced in the temperature curve for different values of A_m and Ω. The variation only affects the boundary condition at the base of the fin, and the nature of the curve soon follows similar trends for different values.
4. The temperature profile in the longitudinal fin increases along Fo and X both as the value of β increases. A higher value of β represents conduction as a prominent phenomenon, resulting in a uniform temperature profile in the fin.
5. The temperature profile in the longitudinal fin decreases when the fin parameter N increases, i.e. the temperature profile is inversely proportional to N. For fast cooling, we require a higher value of the N parameter.
6. An increase in the value of G will result in an increase in ambient heat generation as well as internal heat generation. This will elevate the fin temperature.
7. ε_G increases as the internal heat generation parameter ε increases. This will reduce the heat flux through the fin. As a result, the temperature of the fin will increase, providing an opportunity for hybrid energy system utilisation.

The above study concludes that thermodynamic parameters of the fin, temperature dependent conductivity of fin material, generation number G, and coefficient of internal heat generation play a significant role in releasing internally generated heat of machines into the environment. This research may be expanded to create a mathematical framework combining thermoelectric production in plate fins using simulation to calculate a low-temperature waste energy harvesting system to produce electricity. The developed system will consist of several thermoelectric modules (TEMs) attached to the cooling zone of the Stirling engine, which will provide an opportunity for waste heat utilisation in combination with the Stirling engine power. As a result, the system will incorporate a waste energy channel, a cooling zone, and thermoelectric modules. TEM is placed amid the cooling fins and the waste heat pipes. The temperature differential between the thermoelectric materials hot and cold surfaces will be utilised to transform wasted energy into electrical energy [32,33]. The heat transfer rate provides the researchers with sufficient opportunity to generate electricity utilising ERS. This model can be utilised to design the cold section of the Stirling engine to maintain the desired temperature difference for proper operation.

References

[1] Yang, H.S., Cheng, C.H., & Ali, M.A. (2011). Performance and operating modes of a thermal-lag Stirling engine with a flywheel. *Applied Thermal Engineering*, 205, 118061. doi 10.1016/j.applthermaleng.2022.118061

[2] Kitaya, K., & Isobe, M. (2022). Molecular Dynamics Study of a nano-scale Beta-Type Stirling Engine. *Journal of Pysics: Conference Series*, 2207, 012006. doi: 10.1088/1742-6596/2207/1/012006

[3] McKellar, S. (2016). Atomic hearts: A decade of US government-sponsored development. *Physics Today*, 69(5), 38−44.

[4] Hirata, K., & Kawada, M. (2005). Discussion of Marine Stirling Engine Systems. *Proceedings of the 7th International Symposium on Marine Engineering*, (pp. 1−5), October 24−28, Tokyo, Japan.

[5] Martini, W.R. (1983). *Stirling Engine Design Manual*. 2nd ed. NASA-CR-168088, Martini Engineering, Washington, USA.

[6] Schmidt, G. (1871). Theorie der geschlossenen calorischen maschine. Journal Zeitschrift des Österreichischen Ingenieur- und Architekten-Vereins, p. 79.

[7] Finkelstein, T., Walker, G., & Joschi, J. (1970). Design optimization of Stirling cycle cryogenic cooling engines, *Cryogenic Engineering Conference*, Paper K4, Boulder, Colorado, USA.

[8] Walker, G. (1962). An optimization of the principle design parameters of Stirling-cycle-machines. *Journal of Mechanical Engineering Science*, 4(3). doi: 10.1243/JMES_JOUR_1962_004_032_02

[9] Kirkley, D.W. (1965). A thermodynamic analysis of the Stirling cycle and a comparision with experiment. International Automotive Engineering Congress, Detroit, USA.

[10] Yang, H.S., Ali, M.A., Ravi Teja, K.V., & Yen, Y.F. (2022). Parametric study and design optimization of a kW-class beta-type Stirling engine. *Applied Thermal Engineering*, 215, 119010, doi: 10.1016/j.applthermaleng.2022.119010

[11] Mahkamov, K. (2006). An Axisymmetric Computational Fluid Dynamics Approach to the Analysis of the Working Process of a Solar Stirling Engine. *Journal of Solar Energy Engineering*, 128(1), 45−53, doi: 10.1115/1.2148979

[12] Hung, K.S., & Cheng, C.H. (2010). Numerical Prediction of Flow and Thermal Fields in a Reciprocating Piston-Cylinder Assembly. *Numerical Heat Transfer Part A: Application*, 38(4), 397−421, doi: 10.1080/10407780750022539

[13] Cheng, Ch.H., & Yang, H.S.. (2012). Optimisation of geometrical parameter for Stirling engine based on theoretical Analysis. *Applied Energy*, 92, 395−405, doi: 10.1016/j.apenergy.2011.11.046

[14] Kumaravelu, T., Saadon, S., & Talib, A.R.A. (2021). Heat transfer enhancement of a Stirling engine by using fins attachment in an energy recovery system. *Energy*, 239, 121881, doi: 10.1016/j.energy.2021.121881

[15] Singh, S., Kumar, D., & Rai, K.N. (2013). Wavelet collocation solution for convective radiative continuously moving fin temperature-dependent thermal conductivity. *International Journal of Engineering Advanced Technology*, 2(4), 6−10.

[16] Singh, S., Kumar, D., & Rai, K.N. (2014). Convective - radiative fin with temperature depnedent thermal conductivity, heat transfer coefficient and wavelength dependent surface emissivity.

Propulsion and Power Research, 3(4), 207−221, doi: 10.1016/j.jppr.2014.11.003

[17] Sigh, S., Kumar, D., & Rai, K.N. (2015). Wavelength collocation solution of non-linear Fin problem with temperrature-dependent thermal conductivity and heat transfer coefficient. *International Journal of Nonlinear Analysis and Applications*, 6(1), 105−118. doi: 10.22075/ijnaa.2015.222

[18] Sigh, S., Kumar, D., & Rai, K.N. (2018). Analytical solution of Fourier and non-Fourier heat transfer in longitudinal fin with internal heat generation and periodic boundary condition. *International Journal of Thermal Sciences*, 125, 166−175. doi: 10.1016/j.ijthermalsci.2017.11.029

[19] Faraj, A., Jaber, H., Chahine, K., Faraj, J., Ramadan, M., El Hage, H.E., & Khaled, M. (2020). New Concept of Power Generation Using TEGs: Thermal Modeling, Parametric Analysis and Case Study. *Entropy*, 22(5), 503. doi: 10.3390/e22050503

[20] Buenaventura, G., & Azzopardi, B. (2015). Energy recovery system for retrofitting in internal combustion engine vehicles: A review of techniques. *Renewable and Sustainable Energy Review*, 41, 955−964. doi: 10.1016/j.rser.2014.08.083

[21] Chen, W.H., Chiou, Y.B., Chein, R.Y., Uan, J.Y., & Wang, X.D. (2022). Power generation of thermoelectric generator with plate fins for recovering low-temperature waste heat. *Applied Energy*, 306, 118012. doi: 10.1016/j.apenergy.2021.118012

[22] Ma, J., Sun, Y., & Li, B. (2017). Simulation of combined conductive, convective and radiative heat transfer in moving irregular porous fins by spectral element method. *International Journal of Thermal Sciences*, 118, 475−487. doi: 10.1016/j.ijthermalsci.2017.05.008

[23] Kundu, B., & Lee, K.S. (2013). A Non-Fourier analysis for transmitting heat in fins with internal heat generation. *International Journal of Heat and Mass Transfer*, 64, 1153−1162. doi: 10.1016/j.ijheatmasstransfer.2013.05.057

[24] Aziz, A., & Na, T.Y. (1981). Perturbation analysis for periodic heat transfer in radiating fins. *Wärme- und Stoffübertragung*, 15, 245–253. doi: 10.1007/BF01003645

[25] Ahmadikia, H., & Rismanian, M. (2011). Analytical solution of non-Fourier heat conduction problem on a fin under periodic boundary conditions. *Journal of Mechanical Science and Technology*, 25(11), 2919−2926. doi: 10.1007/s12206-011-0720-5

[26] Aziz, A., & Na, T.Y. (1981). Periodic heat transfer in fins with variable thermal parameters. *International Journal of Heat and Mass Transfer*, 24(8), 1397-1404, doi: 10.1016/0017-9310(81)90189-7

[27] Reader, G.T., & Hooper, C. (1983). *Stirling Engines*. Cambridge: University Press.

[28] Sharma, S.K., & Kumar, D. (2020). A study on Non-Linear DPL Model for Describing Heat Transfer in Skin Tissue during Hyperthermia Treatment. *Entropy*, 22, 481. doi: 10.3390/e22040481

[29] Strikwerda, J.C. (1989). *Finite Difference Schemes and Partial Differential Equations*. Chapman Hall New York.

[30] Bogachki, P., & Shampine, L.F. (1996). An Efficient Runge-Kutta (4,5) Pair. *Computers & Mathematics with Application*, 36(2), 15−28. doi: 10.1016/0898-1221(96)00141-1

[31] Kuosa, M., Saari, K., Kankkunen, A., & Tveit, T.-M. (2012). Oscillating flow in a Stirling engine heat exchanger. *Applied Thermal Engineering*, 45/46, 15−23. doi: 10.1016/j.applthermaleng.2012.03.023

[32] Araoz, J.A., Cardozo, E., Salomon, M., Alejo, L., & Fransson, T.H. (2015). Development and validation of a thermodynamic model for the performance analysis of a gamma Stirling engine prototype. *Applied Thermal Engineering*. 83, 16−30. doi: 10.1016/j.applthermaleng.2015.03.006

[33] Gibson, L., Wilman, E., & Laurance, W. (2017). How green is 'green energy'? *Trends in Ecology & Evolution*, 32(12), 922−935. doi: 10.1016/j.tree.2017.09.007